SUPERCONDUCTORS

10.1126/sciadv.1501652

Real-space localization and quantification of hole distribution in chain-ladder $Sr_3Ca_{11}Cu_{24}O_{41}$ superconductor

Matthieu Bugnet,[1]* Stefan Löffler,[1,2] David Hawthorn,[3] Hanna A. Dabkowska,[4] Graeme M. Luke,[5] Peter Schattschneider,[2] George A. Sawatzky,[6] Guillaume Radtke,[7] Gianluigi A. Botton[1]*

Understanding the physical properties of the chain-ladder $Sr_3Ca_{11}Cu_{24}O_{41}$ hole-doped superconductor has been precluded by the unknown hole distribution among chains and ladders. We use electron energy-loss spectrometry (EELS) in a scanning transmission electron microscope (STEM) at atomic resolution to directly separate the contributions of chains and ladders and to unravel the hole distribution from the atomic scale variations of the O-K near-edge structures. The experimental data unambiguously demonstrate that most of the holes lie within the chain layers. A quantitative interpretation supported by inelastic scattering calculations shows that about two holes are located in the ladders, and about four holes in the chains, shedding light on the electronic structure of $Sr_3Ca_{11}Cu_{24}O_{41}$. Combined atomic resolution STEM-EELS and inelastic scattering calculations is demonstrated as a powerful approach toward a quantitative understanding of the electronic structure of cuprate superconductors, offering new possibilities for elucidating their physical properties.

INTRODUCTION

The quasi–one-dimensional chain-ladder cuprate $Sr_{14-x}Ca_xCu_{24}O_{41}$ has attracted much attention over the past decades for its appealing physical properties. While it is electrically resistive for $x = 0$, it becomes conductive upon Ca doping. A superconducting behavior has been predicted (*1*–*3*) and then experimentally demonstrated (*4*) under high pressure (3 GPa) and at a high doping level ($x = 13.6$). Abbamonte *et al.* (*5*) suggested the existence of a hole Wigner crystal originating from electronic correlations within the hole-doped ladders of the parent compound $Sr_{14}Cu_{24}O_{41}$ (SCO), thereby demonstrating the competition between superconductivity and an insulating phase within the ladders. $Sr_{14-x}Ca_xCu_{24}O_{41}$ is also unique from a structural point of view. In all other cuprate superconductors, copper oxide units are solely arranged in CuO_2 planes. In contrast, $Sr_{14-x}Ca_xCu_{24}O_{41}$ is composed of two alternating stacked copper oxide planes: corner-shared CuO_2 chains and edge-shared Cu_2O_3 ladders interleaved with Sr(Ca) cation planes (Fig. 1). Following the conventional valency rules of Sr and Ca (2+), O (2−), and Cu (2+), there must be missing electrons (added holes) that are responsible for the conductive properties of $Sr_{14-x}Ca_xCu_{24}O_{41}$.

Understanding the physical properties of this chain-ladder compound requires the knowledge of the exact hole distribution within the chains and the ladders. SCO is naturally doped with six holes per formula unit (f.u.), and the total number of holes does not vary with isovalent Ca substitution for Sr. Several estimates of the hole distribution have been reported in literature, using different approaches such as x-ray absorption spectroscopy (XAS) (*6*–*9*), x-ray emission spectroscopy (XES) (*10*), nuclear magnetic resonance (NMR) (*11*, *12*), Hall effect measurements (*13*), infrared reflectivity (*14*), and bond valence sum analysis based on structural coordination data extracted from x-ray (*15*) or neutron (*16*, *17*) diffraction measurements. However, they present a wide disparity as a result of major differences in the interpretation of the results. Most studies indicate that more than 5 holes per f.u. are confined within the chains of SCO and that only a fraction of holes is transferred from the chains to the ladders upon Ca doping. In contrast, the analysis of optical measurements of Osafune *et al.* (*18*) indicates a transfer to ladders of ~2 holes per f.u. upon doping with $x = 11$, a result supported by the bond valence sum analysis of Deng *et al.* (*17*). Finally, O 1*s* XAS analysis indicates an equal distribution of holes among chains and ladders in SCO and the transfer to ladders of more than 1 hole per f.u. upon Ca doping (*7*). Nevertheless, all studies seem to agree on the linear dependence of the hole number in chains (or ladders) on Ca doping.

The vast majority of spectral information available on cuprate superconductors is gathered using probes with spatial resolutions of typically a few micrometers or several hundred nanometers, such as XAS, XES, angular-resolved photoemission spectroscopy, or x-ray photoemission spectroscopy, thus integrating over all Cu-O planes in the structure and making the distinction among the contributions of nonequivalent Cu planes challenging. It should be mentioned that electron energy-loss spectrometry (EELS) has also been used to study the character (*19*, *20*) and symmetry (*21*, *22*) of the hole states in cuprate superconductors with high critical temperature (T_c) but without atomic plane resolution. However, EELS combined with aberration-corrected scanning transmission electron microscopy (STEM) is highly spatially selective. The technique allows the probing of the chemical bonding and the electronic structure at the atomic scale (*23*, *24*) by

[1]Department of Materials Science and Engineering and the Canadian Centre for Electron Microscopy, McMaster University, 1280 Main Street West, Hamilton, Ontario L8S 4M1, Canada. [2]Institute of Solid State Physics and University Service Centre for Transmission Electron Microscopy, Vienna University of Technology, Wiedner Hauptstraße 8-10, A-1040 Vienna, Austria. [3]Department of Physics and Astronomy, University of Waterloo, 200 University Avenue West, Waterloo, Ontario N2L 3G1, Canada. [4]Brockhouse Institute for Materials Research, McMaster University, 1280 Main Street West, Hamilton, Ontario L8S 4M1, Canada. [5]Department of Physics and Astronomy, McMaster University, 1280 Main Street West, Hamilton, Ontario L8S 4M1, Canada. [6]Department of Physics and Astronomy, University of British Columbia, 6224 Agricultural Road, Vancouver, British Columbia V6T 1Z1, Canada. [7]Institut de Minéralogie, de Physique des Matériaux et de Cosmochimie (IMPMC), Sorbonne Universités, Université Pierre et Marie Curie (UPMC), Paris 6, CNRS UMR 7590, Muséum National d'Histoire Naturelle, IRD UMR 206, 4 Place Jussieu, F-75005 Paris, France.
*Corresponding author. E-mail: bugnetm@mcmaster.ca (M.B.); gbotton@mcmaster.ca (G.A.B.)

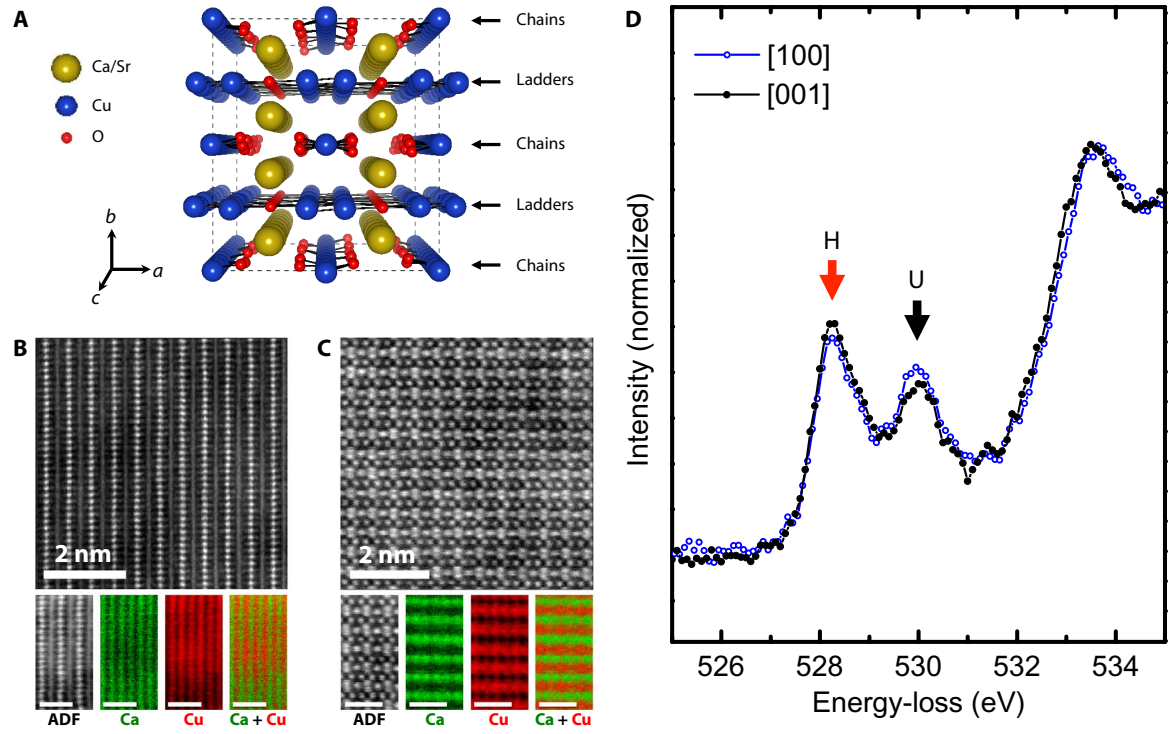

Fig. 1. Crystal structure of SCCO and O-K near-edge structures. (**A**) SCCO structure. (**B** and **C**) Annular dark-field (ADF)–STEM images viewed along the [100] (B) and [001] (C) zone axes. Ca and Cu elemental maps (bottom) were obtained using the Ca-$L_{2,3}$ and Cu-$L_{2,3}$ edges, respectively. Weighted principal component analysis (PCA) was applied to reduce the noise level. Unlabeled scale bars, 1 nm. (**D**) O-K edge onset recorded along the [100] and [001] zone axes. H and U indicate the O 2*p* hole and upper Hubbard band peaks, respectively. The energy resolution was obtained using a monochromator and was comparable to XAS measurements.

using inelastically scattered electrons from a sub-ångström probe and is therefore perfectly suited to separate signals from individual independent Cu planes (*25*–*27*). Furthermore, the energy-loss near-edge structures (ELNES) arising from transitions to unoccupied states of a particular energy allow the mapping of electronic orbitals (*28*) and the localization and identification of the relevant electronic structure information at the atomic scale. Recently, the qualitative real-space mapping of holes has been demonstrated in a series of $YBa_2Cu_3O_{6+\delta}$ compounds (*27*). Whereas a direct visualization of holes can be relevant in itself, the quantification of hole concentrations with atomic resolution is of paramount interest to further understanding the electronic structure and physical properties of hole-doped superconductors from the nano- to the macroscale. To date, this challenge has not been met.

RESULTS

Here, the hole distribution in the chain-ladder superconductor $Sr_3Ca_{11}Cu_{24}O_{41}$ (SCCO) is investigated with STEM-EELS at the atomic level, at room temperature and a pressure of about 10^{-8} mbar, using the O-K pre-edge ELNES (see Fig. 1D). The O-K pre-edge ELNES is composed of the hole band (peak H) associated with the O 2*p* orbitals (*19*, *20*) involved in the Zhang-Rice singlets (*29*) and the upper Hubbard band (peak U). The small anisotropy observed in the monochromated spectra is largely related to the averaging of orientation-dependent effects associated with the use of large convergence and collection angles in STEM-EELS. However, spectral features are in excellent agreement with previous data recorded in polarized XAS (*6*, *7*). Spectrum image (SI) data cubes were recorded with the incident electron beam along the [100] and [001] zone axes of SCCO, simultaneous with the annular dark-field images shown in Fig. 2. After correcting for spatial drift during acquisition (see the Supplementary Materials for details), the spectral information contained in each SI is projected along the direction parallel to the chains and ladders; the data recorded in the [001] zone axis are projected along [100] and vice versa. It is apparent that the O-K fine structures at the edge onset significantly vary from chains to ladders for both specimen orientations: peak H strongly fluctuates as a function of the spatial position, reaching its maximum intensity on the chains and its minimum on the ladders. This observation is further confirmed by a similar experiment at the Cu-L_3 edge (fig. S4), indicating that most holes lie within the CuO_2 chains of the structure.

To evaluate the relative hole concentration within the chains and the ladders, we quantified the spatial variation of the O 2*p* hole band by modeling the O-K pre-edge ELNES. The spatial separation of the chains and ladders achieved using STEM-EELS is highly important because it avoids having to resort to comparison with pure chain and pure ladder reference spectra (*9*), which can induce some material-dependent effects. Gaussian functions have been used to quantify the spectra following the methodology commonly used in XAS (*7*). Note that the present spatially resolved EELS data have been acquired with a lower energy resolution compared to typical XAS experiments, further justifying this choice as a reasonable approximation. Two Gaussian functions were used to fit the O 2*p* hole band and the upper Hubbard band, respectively. The

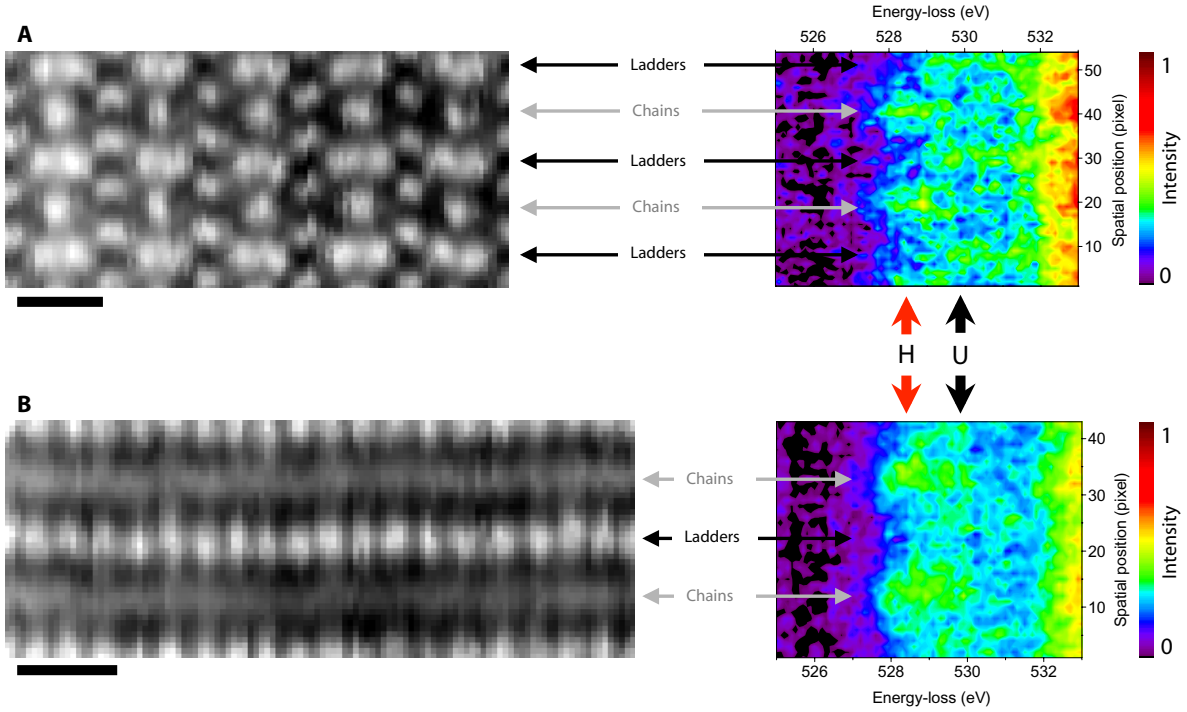

Fig. 2. Qualitative hole distribution. (**A** and **B**) ADF-STEM images and O-K edge onset in the [001] (A) and [100] (B) zone axes. The O-K edge onsets highlight intensity variations of the O 2*p* hole (H) and upper Hubbard (U) bands, whose positions are indicated by red and black arrows, respectively. The ADF-STEM images are represented after alignment (see the Supplementary Materials). Scale bars, 5 Å.

continuum of states at higher energy was modeled by a step function (*30*). The energy of the Gaussian functions was determined after modeling monochromated EELS data, as shown in Fig. 3, B and F, and their full widths at half maximum (FWHM) were evaluated by accounting for the energy resolution decrease between the monochromated and the non-monochromated electron source (see the Supplementary Materials). The spatially resolved data were fitted with the determined energy position and the extrapolated FWHM, leaving the peak intensities as the sole free parameters. It should be mentioned that the independent oxygen sites in chains and in ladders have different O 1*s* core electron binding energies, which would lead to different energies for the doped holes. However, the relative core-level shift estimated from electronic structure calculations in SCO is negligible (*8*), and the experimental chemical shift arising from hole doping in other cuprates such as $La_{2-x}Sr_xCuO_{4-\delta}$ is a few tenths of electron volts for doping levels of a few tenths of holes per Cu (*31*). In comparison with the spectral width of the present experimental peak H (~1.9 eV), the differences in O 1*s* core electron binding energy can be safely neglected.

Examples of the resulting fits of the STEM-EELS data are shown in Fig. 3. The intensity of the Gaussian function used to model the O 2*p* hole peak decreases from chains to ladders, as shown in Fig. 3, C and D, for [001] and Fig. 3, G and H, for [100]. The fitting process was applied to 10 SI data sets acquired in both zone axes. The hole concentrations obtained from this fit are reported in Table 1. Assuming a total of 6 holes per f.u., and that the hole number is directly related to the intensity of peak H with the same spectral weight for ladders and chains, the relative hole concentration within the chains and the ladders along [001] ([100]) is evaluated to be 4.08 ± 0.26 (4.01 ± 0.28) and 1.92 ± 0.26 (1.99 ± 0.28), respectively. As expected, the hole concentrations determined in the [100] and [001] zone axes are similar within the range of error, leading to average values of ~4 holes in the chains and ~2 holes in the ladders, corresponding to ~0.4 hole per Cu in chains and ~0.14 hole per Cu in ladders (considering a 10:14 ratio of Cu atoms in chains/ladders). Accordingly, the upper Hubbard band, which should decrease with higher doping, is weaker in the chains than in the ladders as shown in Fig. 3I. These measurements are consistent with a lower doping per Cu for the ladders, as suggested in $La_{2-x}Sr_xCuO_{4-\delta}$ (*32*).

A reliable quantitative interpretation of the O-K ELNES requires taking into account the channeling of the electron beam along the atomic columns and the relative sensitivity of the O 2*p* hole peak in chains and in ladders (that is, the spectral weight per hole in chains versus ladders). The nearly identical Cu-O interatomic spacing and similar chemistry in chains and ladders suggests that the hole sensitivity of the chains is similar to that of the ladders. To quantitatively evaluate the influences of electron-beam channeling and orientation dependence, we performed inelastic channeling scattering calculations (see the Supplementary Materials for details). The results are summarized in Table 2. On one hand, the inelastic intensity coming from the ladders when the electron beam is on the chains (and vice versa), which we will refer to as cross terms, represents less than ~17% of the total inelastic intensity, which is of the order of experimental uncertainty. In other words, a very good spatial separation of the chain and ladder signals is achieved under these experimental conditions. This result confirms the validity of the experimental STEM-EELS approach used here. On the other hand, these cross terms are of the same magnitude as the small differences in calculated inelastic intensities coming from the chains when the electron beam is in a chain

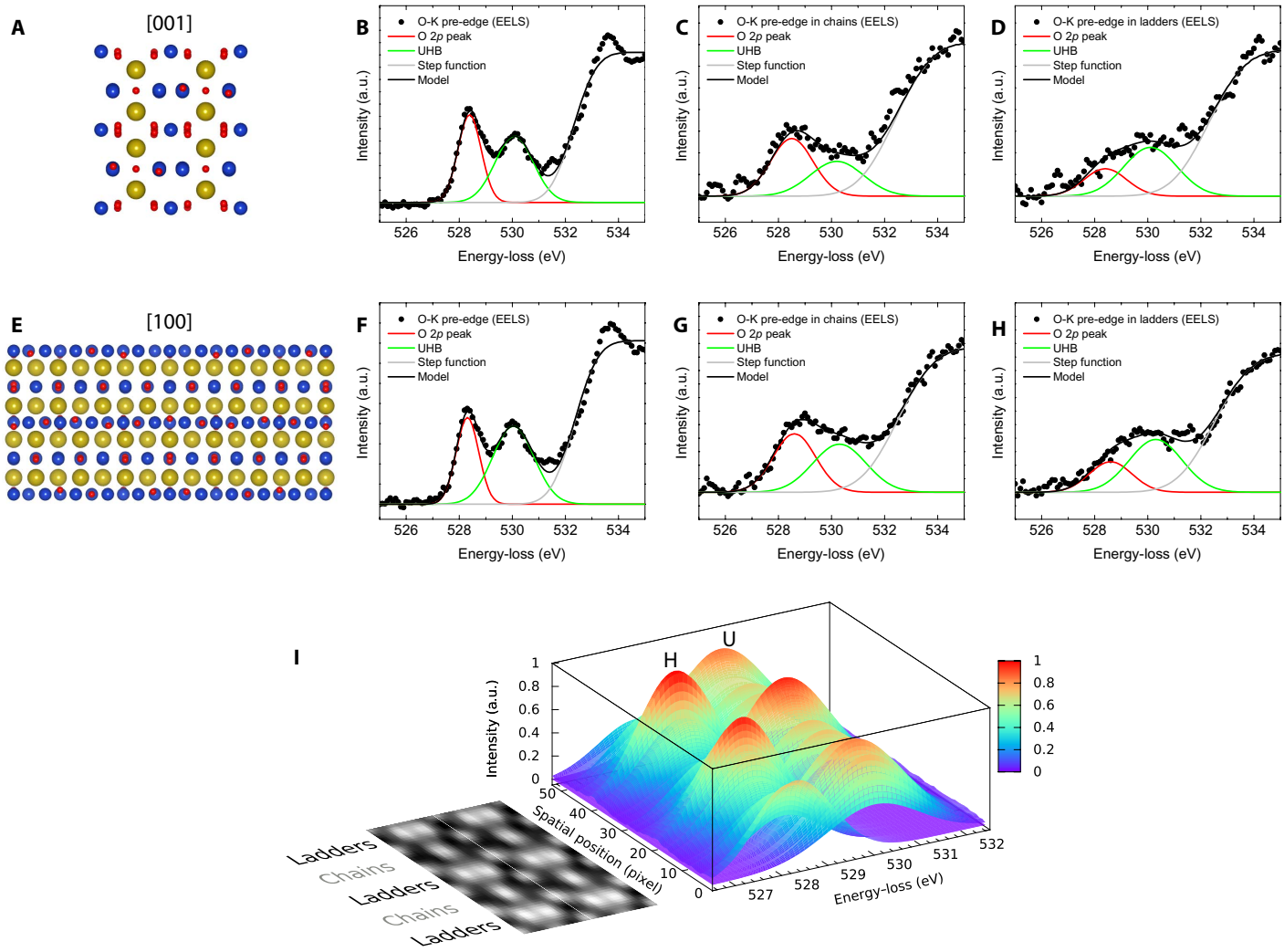

Fig. 3. Spectral fitting and quantitative hole distribution. (**A**) SCCO structure in the [001] zone axis. (**B**) Modeling of the monochromated O-K edge onset in SCCO in the [001] zone axis. (**C**) Modeling of the spatially resolved O-K edge onset in SCCO corresponding to chains in the [001] zone axis. (**D**) Same as in (C) for spectra corresponding to ladders. (**E** to **H**) Same as in (A) to (D) for the [100] zone axis. Two Gaussian functions were used to model the O 2*p* hole band (red solid lines) and the upper Hubbard band (UHB) (green solid lines). The edge onset at higher energy (gray solid lines) was modeled using a step function (*30*). The energy and FWHM of the Gaussian functions were determined from the monochromated spectra in (B) and (F), and only the intensity of the functions was left as free parameters during the fitting process. (**I**) O 2*p* hole band and upper Hubbard band fit over a full spectrum image acquired in the [001] zone axis.

Table 1. Hole concentrations (per f.u.) in chains and ladders. The error bars correspond to the SD over all data sets analyzed and adjustment of the absolute energy positions of the O 2*p* hole band and the upper Hubbard band.

	Ladders	Chains
[100]	1.99 ± 0.28	4.01 ± 0.28
[001]	1.92 ± 0.26	4.08 ± 0.26

position and from the ladders when the electron beam is in a ladder position. This suggests that the O-K ELNES has similar sensitivity to holes in chains and ladders under our experimental conditions and confirms that the expected inelastic intensities recorded in [100] and [001] are comparable.

DISCUSSION

The inelastic channeling calculations confirm the hole concentrations that were directly estimated from Gaussian fitting. First, it is important to highlight that this theoretical approach strongly suggests a spectral weight of 1:1 in chains/ladders, which validates the general assumption made to interpret the XAS data (*6*, *7*). Second, the extracted STEM-EELS data for $x = 11$ are compared with literature values in Fig. 4. Overall, the value of ~2 holes in the ladders follows the general tendency that most of the holes are in the chains upon heavy Ca doping. Specifically, this value is slightly higher than those reported in most of the existing studies (*6*, *9*, *11*, *13*). It is also lower than those extracted from optical measurements (*18*) and neutron diffraction using bond valence sum calculations (*17*). The present study qualitatively and quantitatively shows a higher hole concentration within the chains as compared to the XAS investigation of Rusydi *et al.* (*7*), where it was reported that the holes are

Table 2. Calculated contributions of chains and ladders to the total inelastic intensity.

Orientation	Beam position	Inelastic intensity from ladders (a.u.)	Inelastic intensity from chains (a.u.)
[100]	Ladders	155,956 (~84%)	28,902 (~16%)
	Chains	17,683 (~7%)	240,596 (~93%)
[001]	Ladders	139,527 (~84%)	26,567 (~16%)
	Chains	35,524 (~17%)	177,920 (~83%)

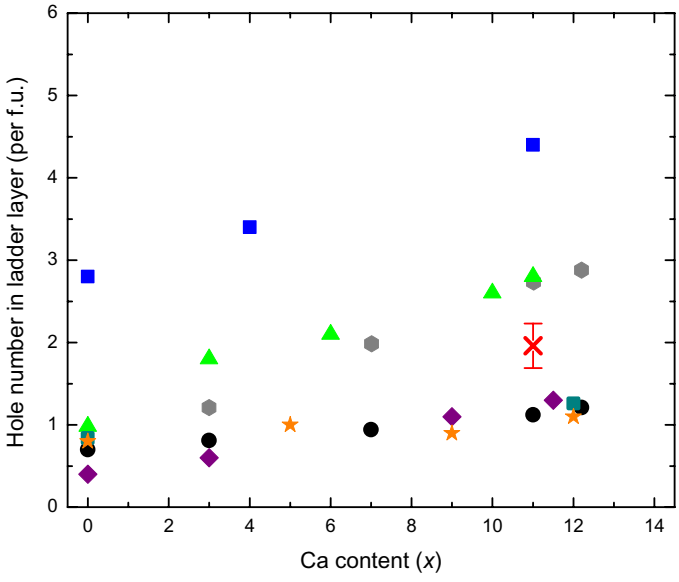

Fig. 4. Hole distribution within the ladders versus Ca content in $Sr_{14-x}Ca_xCu_{24}O_{41}$. The hole distribution from this work (red cross) is indicated in comparison with room-temperature data taken from published works [green triangle: optical measurements, Osafune *et al.* (*18*); orange star: O 1*s* XAS, Nücker *et al.* (*6*); purple diamond: Hall effect, Tafra *et al.* (*13*); black circle: Cu 2*p* XAS, Huang *et al.* (*9*); blue square: O 1*s* XAS, Rusydi *et al.* (*7*); dark cyan square: ^{63}Cu and ^{17}O NMR, Piskunov *et al.* (*11*); gray hexagon: neutron diffraction, Deng *et al.* (*17*)].

mainly localized in the ladders for $x = 11$, inducing a large hole transfer from chains to ladders upon Ca doping. It is important to stress that STEM-EELS coupled to inelastic channeling calculations is the only approach used so far that permits direct visualization and evaluation of hole concentrations in ladders and chains independently, highlighting the relevance and significance of the results reported here.

A major consequence of the STEM-EELS analysis is that the data reveal an apparent incompatibility between the hole distribution in superconducting SCCO and the presence of a hole Wigner crystal in SCO that was suggested by resonant x-ray scattering (*5*) and explained with a nearly equal distribution of holes (*7*) in chains and ladders for $x = 0$. However, note that the Wigner crystallization of holes has been reported on the parent compound ($x = 0$), in contrast to the present STEM-EELS experiments, and this calls for complementary experiments using both STEM-EELS for hole localization and resonant x-ray scattering on a wide range of Ca doping levels. Polarization-dependent work with sufficient spatial resolution to resolve chains and ladders is not possible with current instrumentation, but could be exploited in the future to further understand earlier experiments.

In summary, the hole distribution among chains and ladders in SCCO has been probed by STEM-EELS at atomic resolution. In contrast to XAS and other techniques that probe both chains and ladders simultaneously, STEM-EELS directly distinguishes the signals coming from chains and ladders independently. A qualitative analysis of the results indicates that the chains hold most of the holes. A quantitative analysis is proposed based on the Gaussian fitting of the O-K ELNES pre-edge structures and supported by inelastic channeling calculations, which account for both channeling effects and spectral weight differences in ladders and chains. The combination of the electronic structure fingerprint in the ELNES, atomic resolution in the aberration-corrected STEM, and inelastic scattering calculations opens the way to a better understanding of the electronic properties of cuprate superconductors.

MATERIALS AND METHODS

Crystal growth

Single crystals of SCCO were grown by the optical floating zone (OFZ) method (*33*). The starting materials were pre-annealed powders of $CaCO_3$ (99.9, CERAC), $SrCO_3$ (99.9, AlfaAesar), and CuO (99.9, CERAC). The appropriate stoichiometric mixture of powders was crushed and ground using mortar and pestle to ensure pulverization of the powders and homogeneous mixing, and then the mixture was transferred into a rubber tube. A vacuum pump was used to extract air from the rubber tube, and the material was placed in a hydrostatic press under 60 MPa for 20 min. This produced cylindrical rods of powder that were approximately 11 cm in length and 8 mm in diameter. These rods were sintered in a tube furnace in air for 48 hours at 1200°C and then cooled to room temperature before being removed from the furnace. High-quality single crystals were grown in the OFZ Canon furnace with 9 atm of O_2 overpressure, at a growth rate of 1 mm/hour. The feed and seed rods were counter-rotated at 20 rpm. As SCCO melted incongruently, a flux pellet made of 30 wt % SrO and 70 wt % CuO (0.5 g in total) was used to initiate growth.

Assessment of sample purity and stoichiometry

Energy dispersive x-ray experiments conducted in an FEI Titan 80-300 TEM, operated at 80 kV, confirmed the doping level, with a Sr/Ca content of ~3.1:10.9.

STEM-EELS

The SCCO crystal was oriented by Laue x-ray diffraction. Two specimens, with [100] and [001] orientations, were prepared by focused ion beam (FIB)

cutting using a Zeiss NVision 40 dual beam apparatus. The specimens were subsequently thinned down by ion milling (Fischione Nanomill) at liquid nitrogen temperature with Ar beam energies in the range of 500 to 900 eV to remove the damaged areas from the FIB and to reach electron transparency. The thickness of the areas probed in high-resolution STEM-EELS were determined using EELS (*34*, *35*) as ~30 and ~45 nm in the [100] and [001] zone axes, respectively.

The STEM-EELS experiments were performed on an FEI Titan Cubed 80 300 TEM, equipped with C_s probe and image correctors, operated at 80 kV acceleration voltage, and fitted with a Gatan GIF Quantum Energy Filter. The SI data and the ADF signal were simultaneously acquired with a beam current of ~40 to 50 pA, a convergence semi-angle of 19 mrad, a GIF collection semi-angle of 55 mrad, and a pixel dwell time of 25 ms to maximize the signal while minimizing drift and beam damage artifacts.

Data processing

The elemental atomic resolution maps shown in Fig. 1 were processed by weighted PCA to minimize noise contributions. Data extraction for Figs. 2 and 3 was carried out on raw data. The spatial distortion and drift in the SIs were corrected using a homemade script in the Gatan Digital Micrograph software before projection along one crystallographic direction. See the Supplementary Materials for details. The crystal structure of SCCO is visualized using the computer program VESTA (*36*).

Simulations

Elastic scattering effects were taken into account before and after the inelastic scattering event using the multislice approach. Inelastic scattering was modeled by diagonalizing the mixed dynamic form factor (*37*) obtained from density functional theory calculations (FP-LAPW WIEN2k) (*38*) at the generalized gradient approximation level (*39*). A simplified 224-atom face-centered cubic unit cell, $Ca_{10}Cu_{17}O_{29}$, was used (*40*), assuming x =14 (that is, Sr was fully substituted by Ca), to maintain a reasonable computing time. See the Supplementary Materials for details.

SUPPLEMENTARY MATERIALS

Supplementary material for this article is available at http://advances.sciencemag.org/cgi/content/full/2/3/e1501652/DC1

Comparison with x-ray absorption spectroscopy
Quantitative evaluation of the hole distribution
Inelastic scattering calculations
Drift correction
Qualitative hole distribution from Cu 2*p* excitation
Table S1. Fitting parameters: SD and relative energy positions of Gaussian functions.
Fig. S1. Comparison of O-K XANES and ELNES.
Fig. S2. Inelastic channeling calculations.
Fig. S3. Spatial drift correction on the STEM-EELS data.
Fig. S4. Qualitative hole distribution from Cu 2*p* excitation.

REFERENCES AND NOTES

1. E. Dagotto, J. Riera, D. Scalapino, Superconductivity in ladders and coupled planes. *Phys. Rev. B* **45**, 5744–5767 (1992).
2. E. Dagotto, T. M. Rice, Surprises on the way from one- to two-dimensional quantum magnets: The ladder materials. *Science* **271**, 618–623 (1996).
3. M. Sigrist, T. M. Rice, F. C. Zhang, Superconductivity in a quasi-one-dimensional spin liquid. *Phys. Rev. B Condens. Matter.* **49**, 12058–12061 (1994).
4. M. Uehara, T. Nagata, J. Akimitsu, H. Takahashi, N. Môri, K. Kinoshita, Superconductivity in the ladder material $Sr_{0.4}Ca_{13.6}Cu_{24}O_{41.84}$. *J. Phys. Soc. Jap.* **65**, 2764–2767 (1996).
5. P. Abbamonte, G. Blumberg, A. Rusydi, A. Gozar, P. G. Evans, T. Siegrist, L. Venema, H. Eisaki, E. D. Isaacs, G. A. Sawatzky, Crystallization of charge holes in the spin ladder of $Sr_{14}Cu_{24}O_{41}$. *Nature* **431**, 1078–1081 (2004).
6. N. Nücker, M. Merz, C. A. Kuntscher, S. Gerhold, S. Schuppler, R. Neudert, M. S. Golden, J. Fink, D. Schild, S. Stadler, V. Chakarian, J. Freeland, Y. U. Idzerda, K. Conder, M. Uehara, T. Nagata, J. Goto, J. Akimitsu, N. Motoyama, H. Eisaki, S. Uchida, U. Ammerahl, A. Revcolevschi, Hole distribution in $(Sr,Ca,Y,La)_{14}Cu_{24}O_{41}$ ladder compounds studied by x-ray absorption spectroscopy. *Phys. Rev. B* **62**, 14384–14392 (2000).
7. A. Rusydi, M. Berciu, P. Abbamonte, S. Smadici, H. Eisaki, Y. Fujimaki, S. Uchida, M. Rübhausen, G. A. Sawatzky, Relationship between hole density and charge-ordering wave vector in $Sr_{14-x}Ca_xCu_{24}O_{41}$. *Phys. Rev. B* **75**, 104510 (2007).
8. V. Ilakovac, C. Gougoussis, M. Calandra, N. B. Brookes, V. Bisogni, S. G. Chiuzbaian, J. Akimitsu, O. Milat, S. Tomić, C. F. Hague, Hole depletion of ladders in $Sr_{14}Cu_{24}O_{41}$ induced by correlation effects. *Phys. Rev. B* **85**, 075108 (2012).
9. M.-J. Huang, G. Deng, Y. Y. Chin, Z. Hu, J.-G. Cheng, F. C. Chou, K. Conder, J.-S. Zhou, T.-W. Pi, J. B. Goodenough, H.-J. Lin, C. T. Chen, Determination of hole distribution in $Sr_{14-x}Ca_xCu_{24}O_{41}$ using soft x-ray absorption spectroscopy at the Cu L_3 edge. *Phys. Rev. B* **88**, 014520 (2013).
10. E. Kabasawa, J. Nakamura, N. Yamada, K. Kuroki, H. Yamazaki, M. Watanabe, J. D. Denlinger, S. Shin, R. C. C. Perera, Hole distribution in $(Sr,Ca,Y,La)_{14}Cu_{24}O_{41}$ compounds studied by x-ray absorption and emission spectroscopy. *J. Phys. Soc. Jap.* **77**, 034704 (2008).
11. Y. Piskunov, D. Jérome, P. Auban-Senzier, P. Wzietek, A. Yakubovsky, Hole redistribution in $Sr_{14-x}Ca_xCu_{24}O_{41}$ (x=0,12) spin ladder compounds: ^{63}Cu and ^{17}O NMR studies under pressure. *Phys. Rev. B* **72**, 064512 (2005).
12. K. Magishi, S. Matsumoto, Y. Kitaoka, K. Ishida, K. Asayama, M. Uehara, T. Nagata, J. Akimitsu, Spin gap and dynamics in $Sr_{14-x}Ca_xCu_{24}O_{41}$ comprising hole-doped two-leg spin ladders: Cu NMR study on single crystals. *Phys. Rev. B* **57**, 11533–11544 (1998).
13. E. Tafra, B. Korin-Hamzić, M. Basletić, A. Hamzić, M. Dressel, J. Akimitsu, Influence of doping on the Hall coefficient in $Sr_{14-x}Ca_xCu_{24}O_{41}$. *Phys. Rev. B* **78**, 155122 (2008).
14. S. Frank, A. Huber, U. Ammerahl, M. Hücker, C. A. Kuntscher, Polarization-dependent infrared reflectivity study of $Sr_{2.5}Ca_{11.5}Cu_{24}O_{41}$ under pressure: Charge dynamics, charge distribution, and anisotropy. *Phys. Rev. B* **90**, 224516 (2014).
15. Y. Gotoh, I. Yamaguchi, Y. Takahashi, J. Akimoto, M. Goto, M. Onoda, H. Fujino, T. Nagata, J. Akimitsu, Structural modulation, hole distribution, and hole-ordered structure of the incommensurate composite crystal $(Sr_2Cu_2O_3)_{0.70}CuO_2$. *Phys. Rev. B* **68**, 224108 (2003).
16. M. Isobe, M. Onoda, T. Ohta, F. Izumi, K. Kimoto, E. Takayama-Muromachi, A. W. Hewat, K. Ohoyama, Low-temperature crystal and magnetic structures of the chain-ladder composite material $Sr_{0.4}Ca_{13.6}Cu_{24+y}O_{41+z}$: Hole redistribution and antiferromagnetic order. *Phys. Rev. B* **62**, 11667–11676 (2000).
17. G. Deng, V. Pomjakushin, V. Petříček, E. Pomjakushina, M. Kenzelmann, K. Conder, Structural evolution of one-dimensional spin-ladder compounds $Sr_{14-x}Ca_xCu_{24}O_{41}$ with Ca doping and related evidence of hole redistribution. *Phys. Rev. B* **84**, 144111 (2011).
18. T. Osafune, N. Motoyama, H. Eisaki, S. Uchida, Optical study of the $Sr_{14-x}Ca_xCu_{24}O_{41}$ system: Evidence for hole-doped Cu_2O_3 ladders. *Phys. Rev. Lett.* **78**, 1980–1983 (1997).
19. N. Nücker, J. Fink, J. C. Fuggle, P. J. Durham, W. M. Temmerman, Evidence for holes on oxygen sites in the high-T_c superconductors $La_{2-x}Sr_xCuO_4$ and $YBa_2Cu_3O_{7-y}$. *Phys. Rev. B* **37**, 5158–5163 (1988).
20. J. Fink, J. Fink, N. Nücker, H. Romberg, M. Alexander, S. Nakai, B. Scheerer, P. Adelmann, D. Ewert, Electron energy-loss studies on high-temperature superconductors. *Physica C* **162–164**, 1415–1418 (1989).
21. N. Nücker, H. Romberg, X. X. Xi, J. Fink, B. Gegenheimer, Z. X. Zhao, Symmetry of holes in high-T_c superconductors. *Phys. Rev. B* **39**, 6619–6629 (1989).
22. J. Fink, N. Nücker, E. Pellegrin, H. Romberg, M. Alexander, M. Knupfer, Electron energy-loss and x-ray absorption spectroscopy of cuprate superconductors and related compounds. *J. Electron Spectrosc. Relat. Phenom.* **66**, 395–452 (1994).
23. D. A. Muller, Structure and bonding at the atomic scale by scanning transmission electron microscopy. *Nat. Mater.* **8**, 263–270 (2009).
24. G.-z. Zhu, G. Radtke, G. A. Botton, Bonding and structure of a reconstructed (001) surface of $SrTiO_3$ from TEM. *Nature* **490**, 384–387 (2012).
25. T. Y. Chien, L. F. Kourkoutis, J. Chakhalian, B. Gray, M. Kareev, N. P. Guisinger, D. A. Muller, J. W. Freeland, Visualizing short-range charge transfer at the interfaces between ferromagnetic and superconducting oxides. *Nat. Commun.* **4**, 2336 (2013).
26. G. M. De Luca, G. Ghiringhelli, C. A. Perroni, V. Cataudella, F. Chiarella, C. Cantoni, A. R. Lupini, N. B. Brookes, M. Huijben, G. Koster, G. Rijnders, M. Salluzzo, Ubiquitous long-range antiferromagnetic coupling across the interface between superconducting and ferromagnetic oxides. *Nat. Commun.* **5**, 5626 (2014).
27. N. Gauquelin, D. G. Hawthorn, G. A. Sawatzky, R. X. Liang, D. A. Bonn, W. N. Hardy, G. A. Botton, Atomic scale real-space mapping of holes in $YBa_2Cu_3O_{6+\delta}$. *Nat. Commun.* **5**, 4275 (2014).

28. S. Löffler, Mapping electronic orbitals in real space. *Microsc. Microanal.* **21** (Suppl. S3), 2361–2362 (2015).
29. F. C. Zhang, T. M. Rice, Effective Hamiltonian for the superconducting Cu oxides. *Phys. Rev. B* **37**, 3759–3761 (1988).
30. J. Stöhr, *NEXAFS Spectroscopy* (Springer Science & Business Media, Berlin, 2013) vol. 25.
31. A. Ino, T. Mizokawa, A. Fujimori, K. Tamasaku, H. Eisaki, S. Uchida, T. Kimura, T. Sasagawa, K. Kishio, Chemical potential shift in overdoped and underdoped $La_{2-x}Sr_xCuO_4$. *Phys. Rev. Lett.* **79**, 2101–2104 (1997).
32. C. T. Chen, F. Sette, Y. Ma, M. S. Hybertsen, E. B. Stechel, W. M. C. Foulkes, M. Schulter, S.-W. Cheong, A. S. Cooper, L. W. Rupp Jr., B. Batlogg, Y. L. Soo, Z. H. Ming, A. Krol, Y. H. Kao, Electronic states in $La_{2-x}Sr_xCuO_{4+\delta}$ probed by soft-x-ray absorption. *Phys. Rev. Lett.* **66**, 104–107 (1991).
33. H. A. Dabkowska, A. B. Dabkowski, R. Hermann, J. Priede, G. Gerbet, in *Handbook of Crystal Growth*, T. Nishinaga, P. Rudolph, Eds. (Elsevier, Amsterdam, ed. 2, 2015), vol. 2, pp. 281–329.
34. R. F. Egerton, *Electron Energy-Loss Spectroscopy in the Electron Microscope* (Plenum Press, New York, ed. 2, 1996).
35. T. Malis, S. C. Cheng, R. F. Egerton, EELS log-ratio technique for specimen-thickness measurement in the TEM. *J. Electron Micr. Tech.* **8**, 193–200 (1988).
36. K. Momma, F. Izumi, VESTA: A three-dimensional visualization system for electronic and structural analysis. *J. Appl. Crystallogr.* **41**, 653–658 (2008).
37. S. Löffler, V. Motsch, P. Schattschneider, A pure state decomposition approach of the mixed dynamic form factor for mapping atomic orbitals. *Ultramicroscopy* **131**, 39–45 (2013).
38. P. Blaha, K. Schwarz, G. K. H. Madsen, D. Kvasnicka, J. Luitz, in *Wien2k, An Augmented Plane Wave + Local Orbitals Program for Calculating Crystal Properties*, K. Schwarz, Ed. (Technische Universität Wien, Austria, 2001).
39. J. P. Perdew, K. Burke, M. Ernzerhof, Generalized gradient approximation made simple. *Phys. Rev. Lett.* **77**, 3865–3868 (1996).
40. K. Kato, Strukturverfeinerung des Kompositkristalls im mehrdimensionalen Raum. *Acta Crystallogr. Sect. B: Struct. Sci. B* **46**, 39–44 (1990).

Acknowledgments: M.B. and G.A.B. are grateful to J. Huang and T. Casagrande for sample preparation using FIB and to A. Duft for TEM/STEM maintenance. H.A.D. and G.M.L. thank G. Wright for assistance with the crystal growth experiment. M.B. thanks J. Britten for fruitful discussions. **Funding:** The STEM-EELS work was performed at the Canadian Center for Electron Microscopy, a national facility supported by the Canada Foundation for Innovation under the MSI program, McMaster University, and the Natural Sciences and Engineering Research Council of Canada (NSERC). G.A.B. is grateful to NSERC for supporting this work. D.H., G.M.L., and G.A.S. acknowledge the Canadian Institute for Advanced Research (CIFAR) for research support. G.M.L. acknowledges NSERC for funding of the crystal growth experiment. M.B. acknowledges financial support from the University of British Columbia as a visiting researcher. S.L. acknowledges financial support by the Austrian Science Fund (FWF) under grant number J3732-N27. P.S. acknowledges financial support by the Austrian Science Fund (FWF) under grant number I543-N20. G.R. acknowledges the Institut de Physique (INP) of the French Centre National de la Recherche Scientifique (CNRS) for partial financial support through the International Program for Scientific Cooperation (PICS). **Author contributions:** M.B., G.R., and G.A.B conceived the study and the experiment. H.A.D. performed the crystal growth experiment. M.B. performed the STEM-EELS experiments. M.B., G.R., and S.L. analyzed the data. S.L. performed the channeling simulations. M.B., S.L., and G.R. wrote the manuscript. D.H., P.S., G.A.S., and G.A.B. contributed to data interpretation and the discussions in the manuscript. All authors discussed the results and contributed to the final text of the manuscript. **Competing interests:** The authors declare that they have no competing interests. **Data and materials availability:** All data needed to evaluate the conclusions in the paper are present in the paper and/or the Supplementary Materials. Additional data related to this paper may be requested from the authors.

Submitted 16 November 2015
Accepted 5 February 2016
Published 25 March 2016
10.1126/sciadv.1501652

Citation: M. Bugnet, S. Löffler, D. Hawthorn, H. A. Dabkowska, G. M. Luke, P. Schattschneider, G. A. Sawatzky, G. Radtke, G. A. Botton, Real-space localization and quantification of hole distribution in chain-ladder $Sr_3Ca_{11}Cu_{24}O_{41}$ superconductor. *Sci. Adv.* **2**, e1501652 (2016).